Biomedicine & Pharmacotherapy 95 (2017) 721–730

Contents lists available at ScienceDirect

Biomedicine & Pharmacotherapy

journal homepage: www.elsevier.com/locate/biopha

Original article

Development of 1,3,4-oxadiazole thione based novel anticancer agents: Design, synthesis and in-vitro studies

Nalini Yadav[a], Parveen Kumar[b], Aruna Chhikara[b], Madhu Chopra[a,*]

[a] Laboratory of Anti-cancer Drug Development, Dr. B. R. Ambedkar Center for Biomedical Research, University of Delhi, Delhi 110007, India
[b] Department of Chemistry, Dyal Singh College, University of Delhi, New Delhi 110003, India

ARTICLE INFO

Keywords:
Oxadiazole thiones
Cytotoxicity
G_2-M phase arrest
Apoptosis

ABSTRACT

A series of new 1,3,4-oxadiazole-2(3*H*)-thione analogues (**3a** to **3o**) have been designed, synthesized and evaluated for their anticancer activity. Four different cancerous cell lines viz. HeLa (cervical), U-87 (glioblastoma), Panc (pancreatic) and MCF-7 (breast) were used to assess the potency of the synthesized compounds as anticancer agents. Among them **3i** and **3j** showed promising cytotoxicity against HeLa cell line. Further, **3i** and **3j** successfully inhibited cell cycle progression and displayed cell death in HeLa cells via apoptosis as visualized by Annexin V APC and DNA fragmentation assay. **3i** and **3j** induced caspase-3 activation, PARP cleavage, increase in expression of proapoptotic protein Bax and decrease in the expression of antiapoptotic protein Bcl-2. Also, **3i** and **3j** induced overexpression of p21 and decreased expression of cyclin B1 indicating the arrest of cells in G_2-M phase of the cell cycle. Therefore, new lead compounds are being suggested having anticancer activity through cell cycle inhibition and apoptosis.

1. Introduction

Cancer continues to be major health issue in most parts of the world and is the prominent cause of death world-wide [1]. According to World Health Organization, cancer is the second leading cause of death globally and was responsible for 8.8 million deaths in 2015. Around 70% of deaths from cancer occur in low-income and underdeveloped/developing countries [2]. According to a report from National Cancer Institute, estimated number of cancer deaths in children and teenagers was 1960 in 2014 whereas 15,780 of them were diagnosed with cancer. An individual's risk of developing cancer at any point in his life-time depends on various factors *viz.* age, genetics, and exposure to risk factors which include some potentially avoidable lifestyle habits [3] such as smoking, alcohol, improper and unhealthy diet, insufficient physical activity, obesity, and certain infections which account for a high percentage of cancer cases all over the world [4].

Cancer treatment has been the primary goal of pharmaceutical industries and R & D wings in research centers over the last many decades [5]. Among the various treatment regimens available today, chemotherapy is most commonly used for treating various kinds of cancers worldwide. Serious side effects of the present drug entities, drug resistance and failure of anti-tumor drugs are the main obstacles in successful development of anticancer drugs. Therefore, there is a crucial need for the development of molecules which are endowed with excellent anticancer potency and lower side effects. [6,7]

Oxadiazole are an important class of heterocyclic aromatic compounds with broad spectrum of biological activities such as antibacterial [8], antimycobacterial [9], antifungal [10], anti-HIV [11], anti-inflammatory and analgesic [12–14], hypoglycemic [15], anticonvulsant [16] and anticancer properties [17,18] besides other biological properties such as genotoxic [19] and lipid peroxidation inhibitory activities [20]. 1,3,4-oxadiazole is commonly used moiety for pharmacophore development and has been thoroughly investigated because of its good metabolic profile and hydrogen bonding ability within the receptor site. 1,3,4-oxadiazoles are extremely good bioisosteres of esters and amides, and the presence of azole (−N═C−O) group increases the lipophilicity which facilitates its transportation through cell membranes to reach the target site and show various biological activities [21]. Besides these activities, oxadiazoles (Fig. 1) have also been seen to display excellent anticancer activities in various *in vitro* and *in vivo* models. For example, one of the 2, 3-dihydro-1,3,4-oxadiazole-2-thione derivatives, compound **A** having oxadiazole thione nucleus attached with the phenyl ring showed 73.9% of tumor inhibition on EAC animal models [22]. Another 1,3,4-oxadiazole derivative with an amide group, **B** having oxadiazole moiety showed potent anticancer activity on 4 cancerous cell lines HepG2 (12.4 μg/mL), WI-38 (17.3 μg/mL), VERO (15.8 μg/mL) and MCF-7 (25.80 μg/mL) [23]. In addition one more 3-(1,3,4-oxadiazol) containing compound **C** having

* Corresponding author.
E-mail addresses: mchopradu@gmail.com, mchopra@acbr.du.ac.in (M. Chopra).

http://dx.doi.org/10.1016/j.biopha.2017.08.110
Received 26 July 2017; Received in revised form 21 August 2017; Accepted 24 August 2017

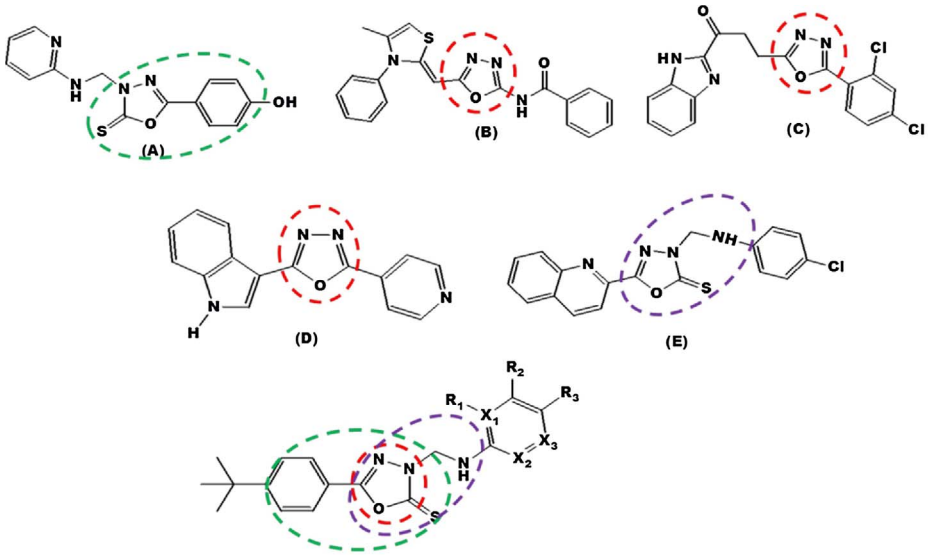

Fig. 1. Design strategy of new derivatives of oxadiazole thiones.

oxadiazole moeity showed excellent antiproliferative effect against full panel of 60 cell lines [24,25]. One of the novel 5-(30-indolyl)-2-(substituted)-1,3,4-oxadiazole containing 4-pyridyl as the −R group substitution, **D** showed excellent cytotoxicity activity against PC3 prostatic cancer cell line [17]. In another series of 2-aminomethyl-5-(quinolin-2-yl)-1,3,4-oxadiazole-2(3H)-thione quinolone derivatives, one of the analogues containing (4-Chlorophenyl) amino moiety **E** displayed very good anticancer activity against HepG2 cell line [26].

During an ongoing programme to develop new, potent and less toxic anticancer compounds and inspired with the diverse biological properties of oxadiazoles and their role in anticancer drug development, we synthesized a series of new 1,3,4-oxadiazole thione derivatives as potent anticancer agents. The 1,3,4-oxadiazole thione core pharmacophore was extended by linking substituted phenyl ring via methylene to study the effect of 'R' group in generating anticancer activity. Synthesized compounds were studied for their cytotoxicity and Structural Activity Relationship (SAR) on 4 cancerous cell lines viz. HeLa, MCF-7, U87 and Panc. The possible mechanism of cytotoxicity action of the most active compounds was further studied through viability staining assays, DNA fragmentation, cell cycle and western blot analysis of key proteins involved in apoptotic pathways as well as cell cycle signaling pathways.

2. Results and discussion

2.1. Chemistry

In the present study, fifteen new mannich bases of 1,3,4-oxadiazole thiones have been designed and synthesized in order to screen for their anticancer activity. The synthesis of compounds **3a** to **3o** followed the general synthetic pathway outlined in Scheme 1. Firstly, 4-(*tert*-butyl) benzohydrazide was reacted with carbon disulphide in the presence of ethanol at 0 °C for 20 min and then refluxed for 4 h until the evolution of H_2S ceased. Retrieved intermediate 5-(4-*tert*-butylphenyl)-1,3,4-oxadiazole-2(3*H*)-thione was purified by column chromatography and further reacted with different amines in the presence of formaldehyde in anhydrous ethanol at room temperature to yield mannich bases of 1,3,4-oxadiazole thiones **3a** to **3o** which were recrystallized from anhydrous ethanol and characterized with ^{1}H NMR, ^{13}C NMR, IR and HRMS.

2.2. Biological evaluation

2.2.1. In vitro antiproliferative activity

All the newly synthesized compounds **3a** to **3o** were evaluated for their antiproliferative activity on 4 cancerous cell lines *viz* HeLa (cervical), U-87 (glioblastoma), Panc (pancreatic) and MCF-7 (breast) using MTT growth inhibition assay [27]. Doxorubicin (**DOX**) was used as positive control. The results are shown in Table 1.

As exhibited in Table 1, compounds **3i** and **3j** bearing nitro and fluoro at the para position of benzene ring respectively, displayed highest activity against HeLa cervical cancer cell line with a half maximal (50%) inhibitory concentration (IC_{50}) value of 7.92 μM and 7.37 μM, respectively after 48 h. **3i** and **3j** showed better antiproliferative activity as compared to earlier reported 5-(Dec-9-enyl)-(3H)-1,3,4-oxadiazol-2-thione and 3-(4-[5-Mercapto-1,3,4-oxadiazole-2-yl] phenylimino)-5-bromo-indolin-2-one which showed IC_{50} value of 11.90 ± 1.3 μM and 10.64 μM respectively on HeLa cells [28,29]. **DOX** showed an IC_{50} value of 1.25 μM against HeLa cell line. SAR studies revealed substitution of methyl groups at the para position **(3a)** or both at the meta and para positions **(3b)** did not increase the potency of the compound and showed 50% inhibitory activity above 27 μM for HeLa, U87 and Panc, owing to electron donating nature of methyl groups. Iodo group at para position **(3c)** displayed good activity on Panc (21.91 ± 1.41 μM), whereas it was slightly less active for U87 and HeLa. Similarly, bromo substitution at the para position **(3d)** displayed good activity against HeLa, Panc and U87 (18.08 ± 1.32 μM) in comparison to its substitution at the ortho position **(3e)** which displayed less activity (> 28 μM) against all the cell lines. Substitution of the chloro group at the para position **(3f)** displayed satisfactory activity against HeLa (23.44 ± 1.20 μM), U87 (22.44 ± 1.25 μM) and Panc (22.80 ± 2.58 μM) while its dual substitution at ortho and meta positions **(3g)** lead to reduction in its cytotoxic activity (> 25 μM) on all the treated cell lines. Ortho nitro substitution **(3h)** was ineffective until a dose of 50 μM on all the tested cell lines, while its para counterpart **(3i)** showed very impressive activity against HeLa (7.92 ± 0.57 μM) and quite good activity against U87 (17.78 ± 1.92 μM) and Panc (20.83 ± 1.15 μM), therefore suggesting that electronegative group is favoured at *p*-position. Substitution of fluoro group at the ortho position **(3k)** displayed less growth inhibitory activity (> 26 μM) against all the four cell lines whereas its substitution on para position **(3j)** showed remarkable growth inhibitory activity against HeLa (7.37 ± 0.50 μM), and good activity (< 20 μM) against U-87 (19.6 ± 1.82 μM) and Panc (12.17 ± 2.47 μM). Above study concludes that halogen or nitro group

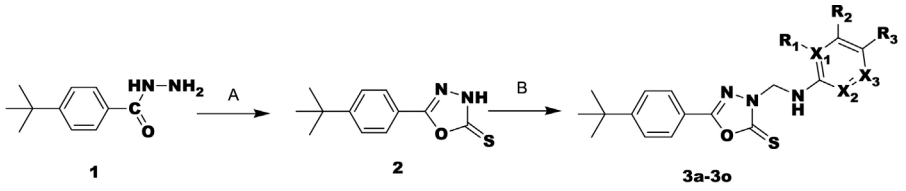

Scheme 1. General scheme for the synthesis of compounds **3a-3o**. Reagents and Conditions: (A) CS_2, KOH, ethanol, 0 °C, 4 h. (B) Amines, HCHO 40%, RT, 4–6 h.

3a	R_1=H; R_2=H; R_3=CH_3; X_1=C; X_2=C; X_3=C	**3i**	R_1=H; R_2=H; R_3=NO_2; X_1=C; X_2=C; X_3=C
3b	R_1=H; R_2= CH_3; R_3= CH_3; X_1=C; X_2=C; X_3=C	**3j**	R_1=H; R_2=H; R_3=F; X_1=C; X_2=C; X_3=C
3c	R_1=H; R_2=H; R_3=I; X_1=C; X_2=C; X_3=C	**3k**	R_1=F; R_2=H; R_3=H; X_1=C; X_2=C; X_3=C
3d	R_1=H; R_2=H; R_3=Br; X_1=C; X_2=C; X_3=C	**3l**	R_1=H; R_2=H; R_3=COOH; X_1=C; X_2=C; X_3=C
3e	R_1=Br; R_2=H; R_3=H; X_1=C; X_2=C; X_3=C	**3m**	R_1=H; R_2=H; R_3=OCH_3; X_1=C; X_2=C; X_3=C
3f	R_1=H; R_2=H; R_3=Cl; X_1=C; X_2=C; X_3=C	**3n**	R_1=H; R_2=H; R_3=H; X_1=C; X_2=C; X_3=N
3g	R_1=Cl; R_2=Cl; R_3=H; X_1=C; X_2=C; X_3=C	**3o**	R_1=H; R_2=H; R_3=H; X_1=N; X_2=N; X_3=C
3h	R_1=NO_2; R_2=H; R_3=H; X_1=C X_2=C; X_3=C		

substitution at the para position of benzene ring increases its activity which might be because of inductive effect of halogens which deactivates the ring. Substitution with carboxylic group at the para position **(3l)** showed satisfactory activity only against Panc (25.64 ± 1.95 μM) and was inactive against all other cell lines tested which could be due to highly polar nature of this compound. Substitution of ethoxy group **(3m)** in the benzene ring also did not increase its potency and IC_{50} obtained for this compound was more than 30 μM because of electron donating nature of lone pairs present on the oxygen of ethoxy group. In last two compounds phenyl groups were replaced with deactivating groups pyridine **(3n)** and pyrimidine **(3o)** rings respectively. The presence of second nitrogen is advantageous in pyrimidine containing compound **3o** (IC_{50} 13.50 ± 2.17 μM) against HeLa cells in comparison to pyridine containing compound **3n** (IC_{50} 32.05 ± 2.92 μM). Overall, MTT results indicate that polar electronegative groups at para position increase the cytotoxicity except in case for carboxylic group which is highly polar. All the oxadiazole thione derivatives reported in this work have been tested on U87 MG (Glioma) and Panc cell lines (pancreatic) for the first time and showed good to moderate overall activity on these cell lines also.

Moreover, all the compounds tested showed less inhibitory effect against breast cancer cell line MCF-7 in comparison to other three cell lines. All the compounds did not show any antiproliferative effect against non-cancerous HEK (Human Embryonic Kidney) cells until 100 μM. The result for noncancerous cell line also has been included in Table 1 and we have also calculated the selectivity index of most active compounds and **DOX** in Table 2. The degree of selectivity (selectivity index, SI) of the most active compounds (**3i** and **3j**) and **DOX** has been presented as the ratio of IC_{50} of the compounds on the normal cell line vs IC_{50} of same compounds on cancerous cell lines. A SI value inferior to 2 may indicate a general toxicity of an extract or a pure compound [30]. In our study we found SI superior to 2 (Table 2) for **3i** (SI = 14.53 for HeLa), **3j** (SI = 15.57 for HeLa) and **DOX** (SI = 62.28 for HeLa) on all the tested cell lines which suggested that the compounds exhibited selectivity against cancer cell lines.

2.2.2. Cellular morphological study

Based on the promising results of **3i** and **3j**, these compounds were further tested for their mechanism of apoptotic activity on HeLa cells. Apoptosis is an active, ATP-dependent process and is characterized by hallmarks such as membrane blebbing, nuclear (essentially, chromatin) condensation, cell shrinkage, internucleosomal DNA fragmentation and protein cleavage [31]. To determine the effect of these compounds on morphology of cells, HeLa cells were treated with the IC_{50} concentrations of **3i** and **3j** for 24 and 48 h and the cells were observed under a phase contrast microscope. The control cells showed regular polygonal or oval shape. Cells underwent remarkable morphological changes such as shrinking, showed membrane blebbing in addition to a few round and floating cells, along with few elongated cells (Fig. S1 in Supplementary file). The number of viable HeLa cells was significantly

Table 1
In vitro anti-proliferative activities of the novel synthesized 1,3,4-oxadiazole thione derivatives (**3a-3o**)[a] on four human cancer cell lines and one normal cell line.

Compounds	HeLa (IC_{50}) μM	U87 (IC_{50}) μM	Panc (IC_{50}) μM	MCF7 (IC_{50}) μM	HEK (IC_{50}) μM
3a	28.95 ± 2.01	28.40 ± 0.95	27.17 ± 1.31	41.76 ± 1.32	185.5 ± 0.69
3b	30.51 ± 1.35	28.36 ± 1.52	27.27 ± 2.02	31.16 ± 2.55	171.7 ± 0.88
3c	27.00 ± 1.09	25.83 ± 1.08	21.91 ± 1.41	39.36 ± 1.77	147.4 ± 0.87
3d	23.60 ± 0.86	18.08 ± 1.32	22.21 ± 1.25	40.79 ± 3.11	137.1 ± 0.40
3e	28.29 ± 2.00	29.47 ± 1.51	28.83 ± 0.63	37.79 ± 2.28	147.2 ± 0.86
3f	23.44 ± 1.20	22.44 ± 1.25	22.80 ± 2.58	40.07 ± 2.27	162 ± 0.46
3g	31.70 ± 1.99	27.86 ± 1.34	25.92 ± 1.21	35.27 ± 2.36	152.7 ± 0.89
3h	> 50	> 50	40.35 ± 2.08	> 50	> 200
3i	7.92 ± 0.57	17.78 ± 1.92	20.83 ± 1.15	35.23 ± 2.22	115.1 ± 0.68
3j	7.37 ± 0.50	19.6 ± 1.82	12.17 ± 2.47	43.08 ± 2.33	114.8 ± 0.75
3k	27.61 ± 4.19	31.18 ± 2.04	26.10 ± 2.93	46.76 ± 1.27	158.5 ± 0.73
3l	31.08 ± 3.08	33.31 ± 2.02	25.64 ± 1.95	45.85 ± 2.45	168.2 ± 0.75
3m	33.17 ± 1.79	31.63 ± 1.39	29.91 ± 3.08	> 50	169.9 ± 0.77
3n	32.05 ± 2.92	31.76 ± 2.54	29.10 ± 2.07	41.71 ± 2.73	145.2 ± 0.55
3o	13.50 ± 2.17	26.20 ± 2.09	23.70 ± 2.42	31.35 ± 1.49	140 ± 0.63
DOX	1.25 ± 0.39	1.58 ± 0.29	1.828 ± 0.31	1.36 ± 0.31	77.86 ± 0.46

[a] The data represented the mean of three experiments in triplicate and were expressed as mean ± SD. The IC_{50} value was represented as the concentration at which 50% survival of cells was observed. Doxorubicin was used as positive control.

Table 2
Selectivity index, SI (IC_{50} of a compound on normal cell line/IC_{50} of the same compound on cancerous cell lines) calculated for **3i, 3j** and **DOX** on four human cancerous cell lines.

	IC_{50} (HEK) (μM)	IC_{50} (HeLa) (μM)	IC_{50} (U87) (μM)	IC_{50} (Panc) (μM)	IC_{50} (MCF7) (μM)
3i	115.1 ± 0.68	7.92 ± 0.57	17.78 ± 1.92	20.83 ± 1.15	35.23 ± 2.22
SI (3i)		14.53	6.47	5.52	3.26
3j	114.8 ± 0.75	7.37 ± 0.50	19.6 ± 1.82	12.17 ± 2.47	43.08 ± 2.33
SI (3j)		15.57	5.85	9.43	2.66
DOX	77.86 ± 0.46	1.25 ± 0.39	1.58 ± 0.29	1.82 ± 0.31	1.36 ± 0.31
SI (DOX)		62.28	49.27	42.78	57.25

reduced after 24 and 48 h of treatment with **3i** and **3j** as compared to untreated cells. Cellular debris was seen in plates treated with **3i, 3j** and **DOX** after 48 h of treatment. These morphological changes in HeLa cells after treatment with **3i** and **3j** clearly showed that cells had undergone stress, stopped multiplying and were showing signs of apoptotic cell death which was more prominent after 48 h of treatment.

2.2.3. Cell migration study

Migration of cancer cells is a fundamental step in tumor progression and metastasis, and the extent of migration ability depends upon the metastatic potential of cancer cells [32]. Migration was determined by enumerating total cells intruding the wound area in control and treated dishes after 24 and 48 h. Photographs were captured at different time intervals i.e. 0, 24 and 48 h. As shown in Fig. S2A in Supplementary file, the number of invasive cervical cancer cells penetrating the wound area was significantly reduced after treatment with **3i**, **3j** and **DOX** as compared to the untreated control group. The number of cells migrated to the wound induced region have been shown in graphical form for each compound in Fig. S2B in Supplementary file. Results of cell migration assay evidently indicate that treatment with **3i** and **3j** might suppress the migration of HeLa cells.

2.2.4. Apoptotic studies

2.2.4.1. Acridine orange/ethidium bromide (AO/EB) staining assay. Viability stains determine the membrane integrity of a cell based on the uptake or exclusion of a dye from the cell [33]. The ethidium bromide/acridine orange stain (EB/AO stain) is a viability stain that detects apoptotic cells. Ethidium bromide is a dye that is only able to pass through the membrane of a dead or dying cell and makes the cell fluoresce red. Acridine orange is membrane-permeable dye that will stain all cells in the sample and makes the cell fluoresce green [34]. HeLa cells were labeled with AO/EB at 24 and 48 h after treatment with **3i**, **3j** and **DOX** and were examined under a fluorescent microscope. Fig. 2 illustrates that after 24 h of treatment, most untreated cells were showing pale green chromatin with organized nuclear structure whereas in **3i**, **3j** and **DOX** treated cells, a few cells were showing condensed or fragmented chromatin and were stained yellowish green or orange.

After 48 h, most of the cells treated with **3i**, **3j** and **DOX** stained orange or red with fragmented chromatin showing the cells in late apoptotic phase in comparison to untreated cells where a very few number of cells stained red. The staining results with AO/EB showed a time dependent increase in the number of cells showing red stained chromatin at their one end which is a hallmark of apoptosis and few of the cells stained totally red, showing necrotic mode of cell death.

2.2.4.2. Annexin-V (APC)/propidium iodide dual staining assay. The apoptotic effect of **3i** and **3j** was further checked by Annexin V (AV)/Propidium iodide (PI) dual staining assay [35]. AV/PI staining helps to examine the occurrence of phosphatidylserine externalization and facilitates the detection of live cells. Our results after staining the treated cells with AV/PI showed that, the percentage of total apoptotic cells significantly increased after 24 and 48 h when treated with these compounds (Fig. 3). The percentage of cells in late apoptotic phase was found to be 11.98%, 6.35% and 12.76% in case of treatment with **3i, 3j** and **DOX** respectively as compared to 0.53% in untreated control cells after 24 h treatment. The percentage apoptotic cells increased to 52.19%, 51.43% and 57.58% in **3i**, **3j** and **DOX** treated cells respectively as compared to 0.94% cells in untreated control cells after 48 h (Table 3). These results confirm a time dependent apoptosis inducing activity of **3i** and **3j** in cervical cancer cells.

2.2.4.3. DNA fragmentation analysis. In apoptotic cells, activated nuclease enzymes cleave the intact DNA in to shorter mononucleosomal fragments. Fragmentation of DNA results in a characteristic DNA ladder like pattern on agarose gel electrophoresis [36]. Thus, DNA fragmentation assay was carried out to further confirm the apoptosis inducing effect of these compounds on HeLa cells. A typical DNA smeared ladder pattern was observed in **3i, 3j** and **DOX** treated lanes. In contrast, there was little or no degradation of DNA from control cells even after 48 h further confirming the apoptotic mode of cell death induced by compounds **3i** and **3j** in HeLa cells

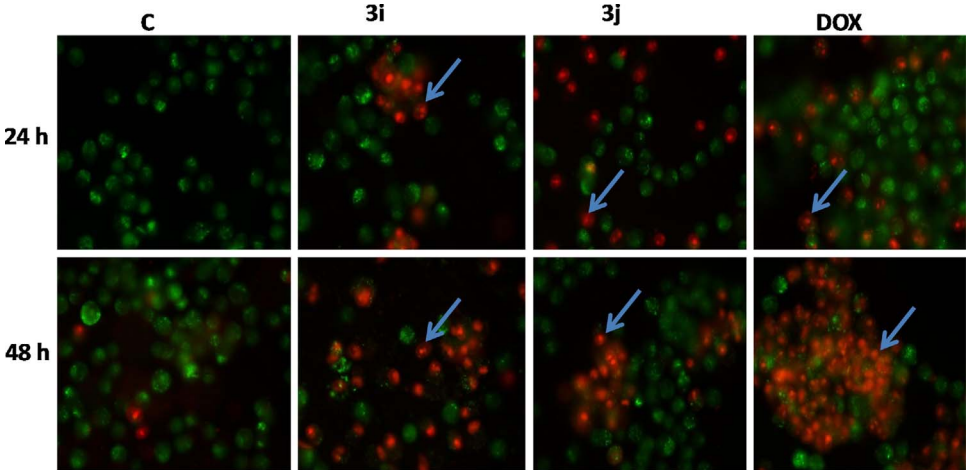

Fig. 2. Acridine Orange/Ethidium Bromide Dual Staining Assay. HeLa cells were treated with IC_{50} concentration of **3i**, **3j** and **DOX** and stained with AO/EtBr after 24 and 48 h and images were captured with a fluorescence microscope. Blue colored arrows indicate apoptotic cells.

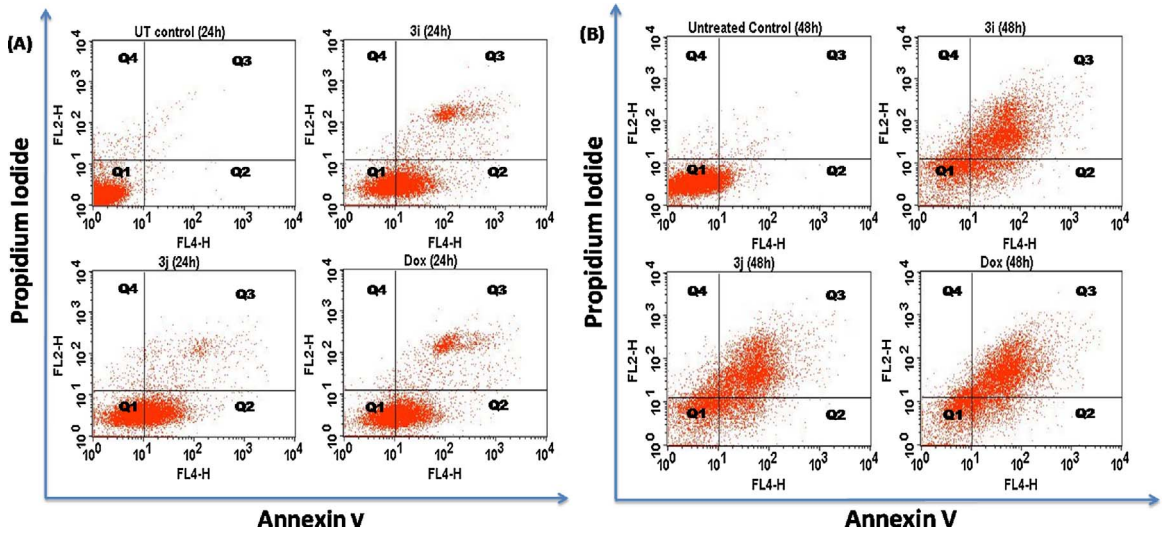

Fig. 3. A and B. Flow cytometric quadrant dot plot of apoptotic HeLa cells after 24 and 48 h treatment respectively with **3i**, **3j** and **DOX**. Apoptosis of HeLa cancer cells as detected by Annexin-V/PI dual staining method.

(Fig. 4A).

2.2.4.4. Western blot analysis. To further elucidate the detailed mechanism of cell death caused by these compounds on HeLa cells the expression levels of caspase 3, PARP, Bax and Bcl-2 which are the key regulators of apoptosis were determined. Induction of apoptosis is accompanied by the activation of several caspases within the same cell [37]. Caspase-3 is an executioner caspase which is activated by both extrinsic (death ligand) or intrinsic (mitochondrial) pathways and is involved in the mass proteolysis which ultimately leads to apoptosis [38]. HeLa cells were treated with DMSO, **3i** and **3j** and the protein was extracted. Our findings revealed that, treated cells showed a decrease in the expression levels of procaspase 3 as compared to control cells and showed expression of cleaved caspase-3 which was absent in control cells indicating that caspase 3 was getting activated after treatment with **3i** and **3j** (Fig. 4B). Caspase-3 is required for the cleavage of ICAD/DFF-45 (inhibitor of caspase-activated DNase) and leads to apoptotic chromatin condensation and DNA fragmentation which concludes in apoptotic cell death [39]. Activated caspase-3 further leads to cleavage of PARP which is an important phenomenon of apoptosis as it prevents the depletion of NAD and ATP which are needed for the later stages of apoptotic process [40]. Presence of cleaved fragment of PARP corresponding to 89 kDa was seen in **3i** and **3j** treated cells whereas there was no expression of cleaved fragment of PARP in untreated cells (Fig. 4B). These results indicate that **3i** and **3j** lead to cell death in HeLa by caspase dependent apoptotic pathway which further leads to DNA fragmentation, chromatin condensation and PARP cleavage. One of the most widely studied negative regulators of apoptosis is the proto-oncogene Bcl-2 whose expression was significantly downregulated in **3i** and **3j** treated cells (Fig. 4B). Expression levels of pro-apoptotic protein Bax increased significantly in the treated lanes. The overall bax/bcl-2 ratio was getting elevated which is critical for the induction of apoptosis and determines whether cells will undergo apoptosis [41,42].

2.2.5. Cell cycle analysis

Many anticancer compounds exert their growth inhibitory effect either by arresting the cell cycle or by induction of apoptosis or a combined effect of both cell cycle arrest and apoptosis [43]. To elucidate the anti-apoptotic mechanism of **3i** and **3j** further, compounds were analyzed to anticipate the phase of cell cycle at which the cells were being arrested. The treatment of HeLa cells with IC_{50} dose of **3i**, **3j** and **DOX** resulted in a decrease in the percentage of cells in the G_1 and S phase and a significant increase in the percentage of cells in G_2 phase. As summarized in table in Fig. 4, the percentage of cells in G_1 phase in untreated cells was 59.30% which reduced to 44.91% in **3i** treated cells, 48.21% in **3j** treated cells and to 7.01% in **DOX** treated cells. The population of cells significantly increased in G_2-M phase i.e. as compared to 20.74% cells in G_2-M phase in untreated control cells, there were approximately 37.25%, 37.87% and 69.66% cells in **3i**, **3j** and **DOX** treated cells, respectively. These results clearly state that the treatment considerably increased the population of cells in G_2 phase after 24 h of treatment as compared to untreated control (Fig. 4D).

2.2.6. Western blot analysis of cell cycle related proteins

Next, we aimed to check the expression of cell cycle related proteins *viz.* p21 and cyclin B1 after treatment with **3i** and **3j** in HeLa cells. p21 is known to prevent proliferation of cells by inhibiting transition between G_1/S and G_2/M phase of the cell cycle as it directly inhibits the

Table 3
Quantitative apoptosis assay of HeLa cells using Annexin-V/PI dual staining method by FACS.[a]

Compounds	Time (h)	Viable Cells (Q_1) %	Early Apoptotic Cells (Q_2) %	Late Apoptotic Cells (Q_3) %	Necrotic Cells (Q_4) %	Apoptotic Cells (Q_2 + Q_3) %
Control	24	97.55 ± 1.19	0.44 ± 0.01	0.53 ± 0.12	1.48 ± 0.16	0.97 ± 0.13
DOX	24	43.30 ± 0.85***	43.43 ± 0.52***	12.76 ± 2.46***	0.51 ± 0.16**	56.19 ± 2.90***
3i	24	43.09 ± 0.48***	44.54 ± 1.64***	11.98 ± 0.72***	0.39 ± 0.14**	56.52 ± 2.09***
3j	24	48.88 ± 0.39***	43.34 ± 0.92***	6.35 ± 1.16**	1.43 ± 0.34^{ns}	49.69 ± 1.92***
Control	48	89.45 ± 0.51	8.80 ± 1.49	0.94 ± 0.22	0.81 ± 0.05	9.74 ± 1.65
DOX	48	22.79 ± 0.98***	14.00 ± 0.70**	57.58 ± 0.96***	5.63 ± 0.78**	71.58 ± 0.91***
3i	48	26.39 ± 0.96***	13.80 ± 0.95**	52.19 ± 0.34***	7.62 ± 0.24***	65.99 ± 0.80***
3j	48	26.18 ± 0.49***	14.17 ± 1.21**	51.43 ± 1.97***	8.22 ± 1.79***	65.60 ± 2.88***

[a] The percentage of viable cells, early apoptotic cells, late apoptotic cells, and necrotic cells are presented as mean ± S.D. (n = 3). ***P < 0.001, **P < 0.01 *vs.* Control of each quadrant for 24 or 48 h. ns = not significant difference as compared to control.

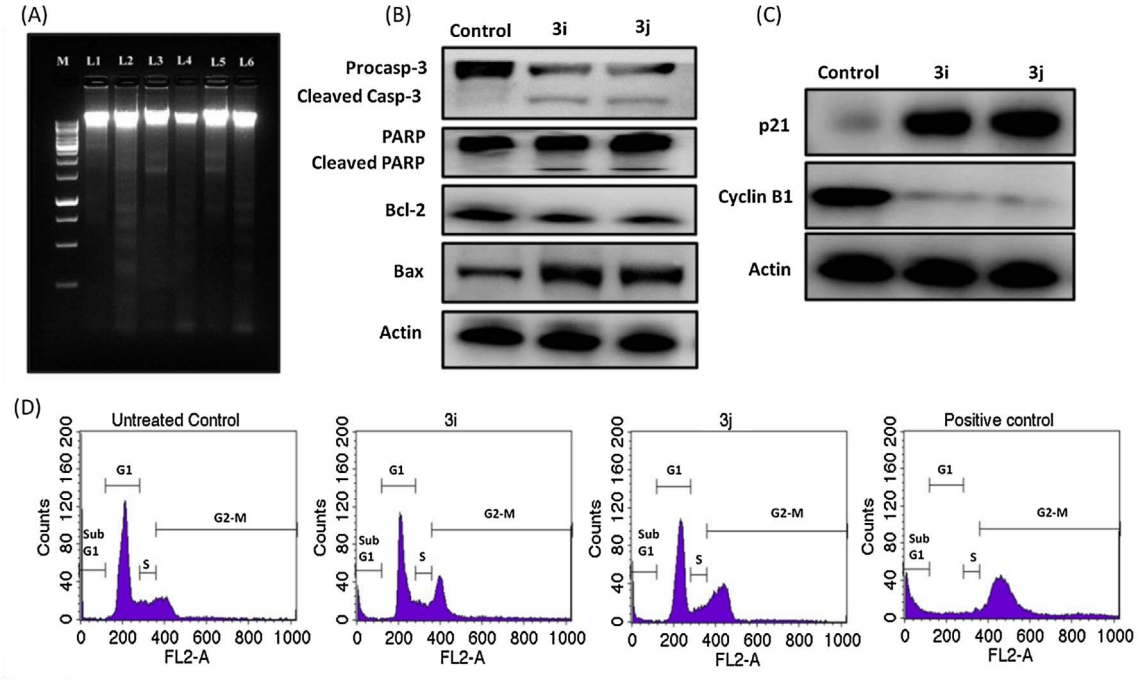

Phases	Control	3i	3j	DOX
G_0	3.95±2.59	4.18±1.28^{ns}	2.95±1.15^{ns}	16.1±4.50**
G_1	59.5±0.21	44.34±0.75***	48.40±0.50***	6.58±0.73***
S	16.98±3.17	10.62±2.68^{ns}	9.28±0.57^{ns}	8.55±6.72^{ns}
G_2	21.12±0.77	39.56±2.15§§§	38.08±1.61§§§	67.92±3.01§§§

Fig. 4. A. Agarose gel electrophoresis of DNA extracted from HeLa cells after treatment with IC_{50} concentration of **3i**, **3j** and doxorubicin for 24 and 48 h. M: DNA ladder; L1: Control (48 h); L2: Doxorubicin (48 h); L3: **3i** (24 h); L4: **3i** (48 h); L5: **3j** (24 h); L6: **3j** (48 h). B. Alteration in the levels of various apoptotic markers *viz.* Caspase-3, PARP, Bcl-2 and Bax after treatment with IC_{50} concentration of **3i** and **3j** for 48 h. C. Change in the levels of proteins p21 and cyclin B1 involved in G_2-M phase of the cell cycle after treatment with IC_{50} concentration of **3i** and **3j** for 48 h. D. Alteration in the percentage of cells in different phases of the cell cycle after treatment with **3i**, **3j** and **DOX** after a period of 24 h. Quantification of cells in different phases of cell cycle in tabular form after treatment with **3i**, **3j** and DOX. Data are presented as mean value ± SD. $^{**}P < 0.01$ for G_0 phase of treated *vs.* control cells; $^{***}P < 0.001$ for G_1 phase of treated *vs.* control cells; $^{§§§}P < 0.001$ for G_2 phase of treated *vs.* control cells; ns = not significant difference for treated *vs.* respective controls.

cyclins and CDKs [44]. As illustrated in Fig. 4C, expression levels of p21 were getting significantly increased in the cells after treatment as compared to control cells. Expression level of cyclin B1 almost diminished in the cells treated with **3i** or **3j**. Cyclin B1 is the regulatory subunit of CDK1 (cdc2), and reduction in the expression level of cyclin B1 can arrest cells in the G_2 phase of the cell cycle and trigger cell death by preventing the chromosomes from condensing and aligning [45]. Thus, this study clearly indicates that HeLa cells were getting arrested in G_2-M phase of the cell cycle after **3i** and **3j** treatment and undergoing apoptosis through caspase dependant pathway.

3. Conclusion

In the present work, fifteen new 5-(4-(*tert*-butyl)phenyl)-1,3,4-oxadiazole-2(3*H*)-thiones have been designed and synthesized by an efficient and convenient synthetic strategy and have been evaluated for their *in vitro* anticancer activity using various assays. Two compounds **3i** and **3j** showed best apoptotic activity on HeLa cervical cancer cells which was better than those of earlier reported oxadiazole derivatives in the literature on the same cell line. None of the synthesized derivatives were showing cytotoxicity against Human Embryonic Kidney (HEK) cells indicating their selectivity against tumor cells. In addition, in our study, the mechanistic details of apoptotic activity was further confirmed through morphological changes induced in the cells after treatment, decrease in the migration of cells in the induced wound area, increased staining of cells with ethidium bromide, induction of phosphatidyl serine externalization, fragmentation of DNA and increase in the bax/bcl2 ratio along with the cleavage of PARP and procaspase-3 proteins. Compounds **3i** and **3j** also profoundly arrested cells in G_2-M phase of the cell cycle in flow cytometry analysis after staining with Propidium Iodide. Western blot analysis of p21 revealed that **3i** and **3j** significantly increased its expression and downregulated the expression of cyclin B1 which is evocative of the potency of **3i** and **3j** to arrest cells in G_2-M phase by targeting these cell cycle regulators. Thus, promising compounds **3i** and **3j** may be considered as a suitable lead for further development of anticancer drugs in future.

4. Experimental

4.1. Chemistry

All the chemicals and reagents were of analytical grade and were purchased from TCI, Sigma-Aldrich, Spectrochem and SD Fine Chemicals Pvt. Ltd. India, and used without further purification. The reactions were monitored using analytical thin layer chromatography (TLC) with silica gel 60–120 (Merck) and F_{254} pre-coated plates (0.25 mm) thickness. Spot on the TLC plates were visualized using ultraviolet light both at short (254 nm) and long wavelength (365 nm) UV light. ^{1}H NMR and ^{13}C NMR spectra were recorded on Jeol 400 MHz nuclear magnetic resonance spectrometers. Chemical shifts are reported in δ (TMS δ, 0.00) or with the solvent reference relative to TMS employed as the internal standard ($CDCl_3$, δ 7.26; DMSO-d_6, δ 3.33) and

multiplicities of NMR signals are designated as s (singlet), d (doublet), t (triplet), q (quartet) and m (multiplet, for unresolved lines). IR spectra of the compounds were recorded on Perkin Elmer FTIR spectrometer (Perkin-Elmer FT-IR Model 9 Spectrophotometer, Singapore). Melting points were obtained on a Kofler apparatus and are uncorrected. HRMS data were collected on Agilent 6520 Q-TOF ESI-HRMS and APCI-HRMS instrument.

4.1.1. General procedure for the synthesis of compound 5-(4-tert-butylphenyl)-1,3,4-oxadiazole-2(3H)-thione (2)

To a solution of 4-(*tert*-butyl)benzohydrazide (**1**) (1.92 g, 0.01 mol) in 25 mL of ethanol at 0 °C, carbon disulphide (2 mL) and potassium hydroxide (0.6 g, 0.01 mol) were added and reaction was refluxed until the evolution of H_2S gas ceased (4 h). Excess solvents were evaporated under reduced pressure and the residue obtained was dissolved in water and then acidified with dilute hydrochloric acid (10%) to pH 5. The precipitate obtained was filtered off, dried and purified by column chromatography on silica gel (eluent: methanol/chloroform = 2: 98) to give compound **2**.

4.1.2. General procedure for the synthesis of compounds (3a-3o)

To a solution of the intermediate (2.0 mmol) (**2**) in ethanol (20 mL), 2.0 mmol of different amines and 10 mmol of HCHO were added and stirred at room temperature for 4–6 h. The residue obtained was filtered and washed with cold ethanol and petroleum ether. The filtrate obtained was dried and crystallized from anhydrous ethanol or acetone to get the compounds **3a** to **3o**.

4.1.3. 5-(4-tert-butylphenyl)-1,3,4-oxadiazole-2(3H)-thione (2)

^{1}H NMR (400 MHz, $CDCl_3$) (δ): White solid, yield: 85%. **^{1}H NMR (400 M*Hz*, $CDCl_3$) (δ)**: 1.34 (s, 9H), 7.51 (d, *J* = 8 *Hz,* 2H*),* 7.865 (d*,* = 12*J* = 12 *Hz,* 2H), 11.36 (s, 1H).

4.1.4. 5-(4-(tert-butyl)phenyl)-3-((4-tolylamino)methyl)-1,3,4-oxadiazole-2(3H)-thione (3a)

White solid, yield: 51.3%, mp: 144–146 °C. **^{1}H NMR (400 M*Hz*, $CDCl_3$) δ:** 1.33 (s, 9H), 2.23 (s, 3H), 5.09 (t, *J* = 8 *Hz*, 1H, NH), 5.51 (d, *J* = 8 *Hz*, 2H), 6.84 (d, *J* = 8 *Hz*, 2H, Ar), 7.02 (d, *J* = 8 *Hz*, 2H, Ar), 7.48 (d, *J* = 8 *Hz*, 2H, Ar), 7.80 (d, *J* = 8 *Hz*, 2H, Ar). **^{13}C (400 M*Hz*, $CDCl_3$) δ**: 20.53, 31.13, 35.26, 59.12, 114.46, 119.60, 126.20, 126.43, 129.31, 130.02, 141.63, 156.25, 159.65, 176.48. **IR (KBr):** 3397.48, 2963.76, 2871.63, 1618.66, 1522.27, 1424.47, 1369.20, 1328.09, 1248.72, 1148.08, 1089.97, 1012.01, 813.58, 761.13, 701.60, 650.58. **HRMS** calculated for $C_{20}H_{23}N_3OS$ $[M+Na]^+$ 376.1460, found $[M+Na]^+$ 376.0417.

4.1.5. 5-(4-(tert-butyl)phenyl)-3-(((3,4-dimethyl)amino)methyl)-1,3,4-oxadiazole-2(3H)-thione (3b)

White solid, yield: 75.7%, mp: 156–158 °C. **^{1}H NMR (400 M*Hz*, $CDCl_3$) δ:** 1.33 (s, 9H), 2.13 (s, 3H), 2.20 (s, 3H), 5.03 (t, *J* = 8 *Hz*, 1H, NH), 5.51 (d, *J* = 8 *Hz*, 2H), 6.70 (d, *J* = 8 *Hz*, 1H), 6.75 (s, 1H), 6.97 (d, *J* = 8 *Hz*, 1H), 7.48 (d, *J* = 8 *Hz*, 2H), 7.80 (d, *J* = 8 *Hz*, 2H). **^{13}C (400 M*Hz*, $CDCl_3$) δ:** 18.82, 20.05, 31.13, 35.25, 59.07, 111.65, 116.14, 119.65, 126.19, 126.41, 128.05, 130.48, 137.74, 141.94, 156.22, 159.64, 176.51. **IR (KBr):** 3431.98, 2969.13, 2370.69, 1627.02, 1525.10, 1383.88, 1272.74, 1160.12, 1118.06, 1089.66, 1042.13, 952.87, 833.58, 764.38. **HRMS** calculated for $C_{21}H_{25}N_3OS$ $[M+K]^+$ 406.2701, found $[M+K]^+$ 406.2113.

4.1.6. 5-(4-(tert-butyl)phenyl)-3-(((4-iodophenyl)amino)methyl)-1,3,4-oxadiazole-2(3H)-thione (3c)

Grayish blue crystalline solid, yield: 52%, mp: 124–126 °C. **^{1}H NMR (400 M*Hz*, $CDCl_3$) δ:** 1.34 (s, 9H), 5.16 (t, *J* = 8 *Hz*, 1H, NH), 5.49 (d, *J* = 8 *Hz*, 2H), 6.72 (d, *J* = 8 *Hz*, 2H, Ar), 7.47 (d, *J* = 8 *Hz*, 2H, Ar), 7.49 (d, *J* = 8 *Hz*, 2H, Ar), 7.81 (d, *J* = 8 *Hz*, 2H, Ar). **^{13}C (400 M*Hz*, $CDCl_3$) δ:** 31.12, 35.28, 58.31, 81.56 116.53, 126.26, 119.41, 126.46, 138.18, 143.87, 156.45, 159.79 176.52. **IR (KBr):** 3381.89, 2960.93, 2870.21, 1618.66, 1591.73, 1505.26, 1424.47, 1454.24, 1367.78, 1245.88, 1190.60, 1146.66, 1094.22, 1007.76, 815.00, 756.88, 698.77. **HRMS** calculated for $C_{19}H_{20}IN_3OS$ $[M+Na]^+$ 488.0270, found $[M+Na]^+$ 489.1379

4.1.7. 3-(((4-bromophenyl)amino)methyl)-5-(4-(tert-butyl)phenyl)-1,3,4-oxadiazole-2(3H)-thione (3d)

White shiny crystalline solid, yield: 73%, mp: 166–168 °C. **^{1}H NMR (400 M*Hz*, $CDCl_3$) δ**: 1.34 (s, 9H), 5.16 (t, *J* = 8 *Hz*, 1H, NH), 5.50 (d, *J* = 8 *Hz*, 2H), 6.81 (d, *J* = 12 *Hz*, 2H), 7.31 (d, *J* = 8 *Hz*, 2H), 7.49 (d, *J* = 8 *Hz*, 2H), 7.81 (d, *J* = 8 *Hz*, 2H). **^{13}C (400 M*Hz*, $CDCl_3$) δ:** 31.16, 35.31, 58.53, 112.05, 116.05, 119.44, 126.30, 126.49, 132.34, 143.23, 156.48, 159.82, 176.55. **IR (KBr):** ν (cm^{-1}) 3316.69, 2962.34, 2904.03, 2870.21, 1665.43, 1618.66, 1593.14, 1510.93, 1455.66, 1372.35, 1319.59, 1250.13, 1189.19, 1149.50, 1088.55, 1010.60, 817.83, 759.72, 697.35, 643.49. **HRMS** calculated for $C_{19}H_{20}BrN_3OS$ $[M+K]^+$ 456.1493, found $[M+K]^+$ 456.1350.

4.1.8. 3-(((2-bromophenyl)amino)methyl)-5-(4-(tert-butyl)phenyl)-1,3,4-oxadiazole-2(3H)-thione (3e)

Off-white shiny crystalline solid, yield: 75%, mp: 109–111 °C. **^{1}H NMR (400 M*Hz*, $CDCl_3$) δ**: 1.33 (s, 9H), 5.59 (d, *J* = 8 *Hz*, 2H), 5.71 (t, *J* = 8 *Hz*, 1H, NH), 6.67-6.71 (m, 1H, Ar),7.22 (d, *J* = 4 *Hz*, 2H, Ar),7.43 (d, *J* = 8 *Hz*, 1H, Ar),7.49 (d, *J* = 8 *Hz*, 2H, Ar),7.82 (d, *J* = 8 *Hz*, 2H, Ar). **^{13}C (400 M*Hz*, $CDCl_3$) δ:** 31.16, 35.31, 58.02, 110.74, 113.35, 119.50, 120.67, 126.28, 126.52, 128.77, 132.96, 141.53, 156.44, 159.85, 176.54**. IR (KBr):** 3405.99, 2962.34, 2904.23, 2871.63, 1598.81, 1510.93, 1423.06, 1408.88, 1250.13, 1149.50, 1097.06, 1019.10, 841.93, 751.21, 701.60, 659.08. **HRMS** calculated for $C_{19}H_{20}BrN_3OS$ $[M+K]^+$ 456.1493, found $[M+K]^+$ 456.1458.

4.1.9. 5-(4-(tert-butyl)phenyl)-3-(((4-chlorophenyl)amino)methyl)-1,3,4-oxadiazole-2(3H)-thione (3f)

White solid, yield: 76%, mp: 181–184 °C. **^{1}H NMR (400 M*Hz*, $CDCl_3$) (δ)**: 1.33 (s, 9H), 5.16 (t, *J* = 8 *Hz*, 1H, NH), 5.50 (d, *J* = 8 *Hz*, 2H), 6.86 (d, *J* = 8 *Hz*, 2H), 7.17 (d, *J* = 8 *Hz*, 2H), 7.49 (d, *J* = 12 *Hz*, 2H), 7.81 (d, *J* = 8 *Hz*, 2H). **^{13}C (400 M*Hz*, $CDCl_3$) δ**: 31.15, 35.31, 58.67, 115.60, 119.45, 124.86, 126.49, 129.45, 142.76, 156.48, 159.81, 176.55. **IR (KBr)**: 3318.11, 2966.60, 2902.81, 2871.63, 1620.07, 1608.75, 1598.81, 1519.14, 1496.76, 1431.56, 1374.86, 1329.51, 1264.31, 1087.13, 1034.69, 1012.01, 826.33, 762.55, 698.77, 653.41. **HRMS** calculated for $C_{19}H_{20}ClN_3OS$ $[M]^+$ 373.1015, found $[M]^+$ 373.0523.

4.1.10. 5-(4-(tert-butyl)phenyl)-3-(((2,3-dichlorophenyl)amino)methyl)-1,3,4-oxadiazole-2(3H)-thione (3g)

White shiny crystalline solid, yield: 71.3%, mp: 164–166 °C. **^{1}H NMR (400 M*Hz*, $CDCl_3$) δ:** 1.33 (s, 9H), 5.58 (d, *J* = 8 *Hz*, 2H, CH_2), 5.82 (t, *J* = 8 *Hz*, 1H, NH), 6.91 (d, *J* = 8 *Hz*, 1H, Ar), 7.08-7.16 (m, 2H, Ar), 7.49 (d, *J* = 8 *Hz*, 2H, Ar), 7.81 (d, *J* = 8 *Hz*, 2H, Ar). **^{13}C (400 M*Hz*, $CDCl_3$) δ**: 31.33, 35.29, 57.73, 111.14, 118.64, 119.36 120.84, 126.28, 126.51, 128 133.42 142.18, 156.53, 159.92, 176.54. **IR (KBr):** 3424.41, 2962.34, 2870.21, 1618.66, 1588.89, 1505.26, 1423.06, 1369.20, 1304.00, 1255.80, 1201.94, 1116.90, 1040.36, 1012.01, 840.51, 761.13, 700.19, 659.08. **HRMS** calculated for $C_{19}H_{19}Cl_2N_3OS$ $[M+Na]^+$ 430.0524, found $[M+Na]^+$ 430.0589.

4.1.11. 5-(4-(tert-butyl)phenyl)-3-(((2-nitrophenyl)amino)methyl)-1,3,4-oxadiazole-2(3H)-thione (3h)

Mustard yellow solid, yield: 42%, mp: 174–176 °C. **^{1}H NMR (400 M*Hz*, $CDCl_3$) δ:** 1.33 (s, 9H), 5.68 (d, *J* = 8 *Hz*, 2H, NH), 6.85 (t, *J* = 8 *Hz*, 1H), 7.48-7.55 (m, 4H, Ar), 7.82 (d, *J* = 8 *Hz*, 2H, Ar), 8.20 (d, *J* = 8 *Hz*, 1H), 8.82 (d, *J* = 8 *Hz*, 1H, Ar). **^{13}C (400 M*Hz*, $CDCl_3$) δ**: 31.11, 35.29, 56.56, 115.24, 118.46, 119.24, 126.29, 126.53, 126.99, 133.92, 136.57, 142.26, 156.64, 160.10, 176.56. **IR (KBr):** 3381.89,

2960.93, 2870.21, 1614.40, 1577.55, 1506.68, 1423.06, 1340.85, 1244.46, 1167.93, 1095.64, 1060.20, 840.51, 748.38, 697.35, 627.90. **HRMS** calculated for $C_{19}H_{20}N_4O_3S$ $[M+Na]^+$ 407.1154, found $[M+Na]^+$ 407.1151.

*4.1.12. 5-(4-(tert-butyl)phenyl)-3-(((4-nitrophenyl)amino)methyl)-1,3,4-oxadiazole-2(3H)-thione (**3i**)*

Light brown solid, yield: 72%, mp: 174–176 °C. **^{1}H NMR (400 M*Hz*, $CDCl_3$) δ:** 1.33 (s, 9H), 5.58 (d, J = 8 *Hz*, 2H), 5.79 (t, J = 8 *Hz*, 1H, NH), 6.97 (d, J = 8 *Hz*, 2H, Ar), 7.50 (d, J = 8 *Hz*, 2H, Ar), 7.81 (d, J = 8 *Hz*, 2H, Ar), 8.13 (d, J = 8 *Hz*, 2H, Ar). **^{13}C (400 M*Hz*, $CDCl_3$) δ**: 31.10, 35.31, 57.32, 113.24, 119.17, 126.24, 126.34, 126.50, 140.54, 150.01, 156.74, 159.98, 176.65. **IR (KBr):** 3376.22, 2963.76, 2904.23, 2873.05, 1600.23, 1506.68, 1424.47, 1373.45, 1325.26, 1257.22, 1190.60, 1148.08, 1106.98, 1010.63, 840.51, 756.88, 697.35, 643.49. **HRMS** calculated for $C_{19}H_{20}N_4O_3S$ $[M+Na]^+$ 407.1154, found $[M+Na]^+$ 407.1156.

*4.1.13. 5-(4-(tert-butyl)phenyl)-3-(((4-fluorophenyl)amino)methyl)-1,3,4-oxadiazole-2(3H)-thione (**3j**)*

White crystalline solid, yield: 65%, mp: 76–78 °C. **^{1}H NMR (400 M*Hz*, $CDCl_3$) (ppm):** 1.33 (s, 9H), 5.09 (t, J = 8 *Hz*, 1H, NH), 5.49 (d, J = 8 *Hz*, 2H), 6.84-6.94 (m, 4H), 7.49 (d, J = 8 *Hz*, 2H), 7.81 (d, J = 8 *Hz*, 2H, Ar). **^{13}C (400 M*Hz*, $CDCl_3$) δ**: 31.12, 35.27, 59.32, 115.53, 115.60, 115.95, 116.17, 119.46, 126.25, 126.44, 140.23, 156.04, 156.41, 158.40, 159.76, 176.50. **IR (KBr):** 3367.72, 2963.76, 2905.65, 2871.63, 1615.82, 1513.77, 1424.47, 1367.78, 1309.66, 1251.55, 1223.20, 1146.66, 1092.80, 1012.01, 829.17, 759.72, 701.60, 649.16. **HRMS** calculated for $C_{19}H_{20}FN_3OS$ $[M+Na]^+$ 380.1209, found $[M+Na]^+$ 380.1171.

*4.1.14. 5-(4-(tert-butyl)phenyl)-3-(((2-fluorophenyl)amino)methyl)-1,3,4-oxadiazole-2(3H)-thione (**3k**)*

White crystalline solid, yield: 76%, mp: 88–90 °C. **^{1}H NMR (400 M*Hz*, $CDCl_3$) δ:** 1.33 (s, 9H), 5.37 (t, 1H, NH), 5.57 (d, J = 8 *Hz*, 2H), 6.75-6.77 (m, 1H), 6.97-7.06 (m, 2H), 7.23 (t, J = 8 *Hz*, 1H, Ar), 7.49 (d, J = 8 *Hz*, 2H, Ar), 7.81 (d, J = 8 *Hz*, 2H, Ar). **^{13}C (400 M*Hz*, $CDCl_3$) δ**: 31.12, 35.27, 57.92, 114.16, 115.05, 115.24, 119.68, 119.75, 124.77, 124.80, 126.24, 126.47, 132.56, 132.67, 150.72, 153.10, 156.40, 159.80, 176.55. **IR (KBr):** 3411.66, 2963.76, 1620.07, 1520.86, 1454.24, 1370.61, 1254.39, 1194.86, 1094.22, 1040.36, 1013.43, 839.09, 751.21, 701.60. HRMS calculated for $C_{19}H_{20}FN_3OS$ $[M+Na]^+$ 380.1209, found $[M+Na]^+$ 380.1183

*4.1.15. 4-(((5-(4-(tert-butyl)phenyl)-2-thioxo-1,3,4-oxadiazol-3(2H)-yl) methyl)amino)benzoic acid (**3l**)*

White crystalline solid, yield: 42%, mp: 208–210 °C. **^{1}H NMR (400 M*Hz*, $CDCl_3$) δ:** 1.33 (s, 9H), 5.23 (t, J = 8 *Hz*, 1H, NH), 5.55 (d, J = 8 *Hz,* 2H), 7.14 (d, J = 8 *Hz*, 1H), 7.32 (d, J = 8 *Hz,* 1H, Ar), 7.49 (d, J = 8 *Hz,* 2H, Ar), 7.81 (d, J = 8 *Hz,* 2H, Ar), 8.08 (d, J = 8 *Hz,* 1H, Ar), 8.27 (d, J = 4 *Hz,* 1H, Ar). **^{13}C (400 M*Hz*, DMSO) δ**: 31.25, 35.44, 57.75, 112.80, 119.70, 120.29, 126.43, 126.62, 126.93, 131.58, 150.19, 156.24, 159.51, 167.75, 176.06. **IR (KBr):** 3357.80, 2963.761, 1678.19, 1605.90, 1254.39, 1179.26, 1101.31, 841.93, 765.391, 698.77. **HRMS** calculated for $C_{20}H_{21}N_3O_3S$ $[M+1]^+$ 384.1383, found $[M+1]^+$ 384.3089.

*4.1.16. 5-(4-(tert-butyl)phenyl)-3-(((4-ethoxyphenyl)amino)methyl)-1,3,4-oxadiazole-2(3H)-thione (**3m**)*

Bluish white solid powder, yield: 40%, mp: 78–80 °C. **^{1}H NMR (400 M*Hz*, $CDCl_3$) δ:** 1.30 (s, 9H), 1.31 (t, J = 8 *Hz*, 3H), 3.88-3.93 (q, 2H), 4.92 (t, J = 8 *Hz*, 1H, NH), 5.45 (d, J = 8 *Hz*, 2H), 6.74 (d, J = 8 *Hz*, 2H, Ar), 6.82 (d, J = 8 *Hz*, 2H, Ar), 7.45 (d, J = 8 *Hz*, 2H, Ar), 7.77 (d, J = 8 *Hz*, 2H, Ar). **^{13}C (400 M*Hz*, $CDCl_3$) δ**: 15.02, 31.13, 35.26, 59.85, 63.94, 115.72, 115.90, 119.58, 126.21, 126.43, 137.66, 153.09, 156.27, 159.66, 176.45. **IR (KBr):** 3390.40, 2966.60, 2902.81, 2873.05, 1618.66, 1515.19, 1421.64, 1367.78, 1234.54, 1146.66, 1091.39, 922.72, 826.33, 756.88, 703.43. **HRMS** calculated for $C_{21}H_{25}N_3O_2S$ $[M+1]^+$ 384.1746, found $[M+1]^+$ 384.1741.

*4.1.17. 5-(4-(tert-butyl)phenyl)-3-((pyridin-3-ylamino)methyl)-1,3,4-oxadiazole-2(3H)-thione (**3n**)*

White crystalline solid, yield: 73%, mp: 162–164 °C. **^{1}H NMR (400 M*Hz*, $CDCl_3$) δ**: 1.33 (s, 9H), 5.23 (t, J = 8 *Hz*, 1H, NH), 5.55 (d, J = 8 *Hz*, 2H), 7.13-7.16 (q, J = 4 *Hz*, 1H, Ar), 7.31-7.33 (m, 1H, Ar), 7.49 (d, J = 8 *Hz*, 2H, Ar), 7.81 (d, J = 8 *Hz*, 2H, Ar), 8.08 (d, J = 4 *Hz*, 2H, Ar), 8.27 (d, J = 4 *Hz*, 2H, Ar). **^{13}C (400 M*Hz*, $CDCl_3$) d:** 31.11, 35.28, 58.15, 119.32, 120.51, 123.95, 126.27, 126.47, 137.37, 140.52, 141.31, 156.52, 159.85, 176.57. **IR (KBr):** 3254.33, 2960.93, 1617.24, 1590.31, 1370.61, 1423.06, 1262.89, 1097.06, 1013.43, 843.34, 758.30, 704.44. **HRMS** calculated for $C_{18}H_{20}N_4OS$ $[M+1]^+$ 341.1437, found $[M+1]^+$ 341.1674.

*4.1.18. 5-(4-(tert-butyl)phenyl)-3-((pyrimidin-2-ylamino)methyl)-1,3,4-oxadiazole-2(3H)-thione (**3o**)*

White Powder, yield: 78%, mp: 176–178 °C. **^{1}H NMR (400 M*Hz*, $CDCl_3$) δ:** 1.33 (s, 9H), 5.83 (d, J = 8 *Hz*, 2H), 6.35 (t, J = 8 *Hz*, 1H), 6.71 (1, J = 4 *Hz*, 1H), 7.48 (d, J = 8 *Hz*, 2H), 7.83 (d, J = 12 *Hz*, 2H), 8.39 (d, J = 8 *Hz*, 2H, Ar). **^{13}C (400 M*Hz*, $CDCl_3$) δ**: 31.12, 35.25, 55.69, 113.04, 119.56, 126.16, 126.49, 156.23, 158.37, 159.55, 161.05, 176.68. **IR (KBr):** 3251.49, 2963.76, 2871.63, 1587.47, 1530.78, 1415.97, 1373.45, 1262.89, 1141.00, 1038.94, 1010.60, 840.51, 759.72, 700.19. **HRMS** calculated for $C_{17}H_{19}N_5OS$ $[M+1]^+$ 342.1389, found $[M+1]^+$ 342.1383.

4.2. Biological evaluation

4.2.1. Cell proliferation assay

U87, HeLa, Panc and MCF-7 cells (3000 cells per well) were cultured and seeded into 96-well plates. After overnight incubation, the cells were treated with compounds **3a** to **3o** at different concentrations (0.1 μM to 100 μM) at 37 °C in an atmosphere of 5% CO_2 for 48 h. Doxorubicin (**DOX**) was used as positive control. The concentration of DMSO used to dissolve the fractions did not exceed 0.3%. Cell viability was determined by using MTT assay (Mosmann et al., December 1983). Following treatment, MTT dye (3-(4, 5 dimethylthiazol-2-yl)-2, 5-diphenyltetrazolium bromide) (Himedia, Mumbai, India) solution in PBS (5 mg/mL) was added and incubated in a CO_2 incubator for 4 h. Formazan crystals formed were dissolved in DMSO and absorbance was measured by using the microplate reader (Tecan, Genios-Pro) at 570 nm. Cell viability of treated cells was calculated in reference to the vehicle control cells using the formula as viability (%) = [100 * (Sample Abs)/(Control Abs)], where Abs is the absorbance value at 570 nm.

4.2.2. Morphological analysis

Appropriate number of HeLa cells was seeded in to 6 well plates for 24 and 48 h treatment with **3i**, **3j** and **DOX**. The morphology of the cells was observed in inverted phase contrast microscope (Nikon, Eclipse TE 2000, Japan) after 24 and 48 h of treatment at a focus of 10× and the images were captured using NIS elements software.

4.2.3. Cell migration study

HeLa cells were seeded into 6-well culture plates with serum-containing medium and were cultured until the cell density reached ~80% confluency. After 24 h of incubation, an artificial homogeneous wound was created by scratching the monolayer with a sterile 200 μL pipette tip. After scratching, the cells were washed with serum-free medium and treated with **3i**, **3j** and **DOX**. Images of the cells migrated into the wound induced area were captured at a period of 0, 24 and 48 h using NIS element software. The assay was performed in triplicates.

4.2.4. Acridine orange/ethidium bromide (AO/EB) staining assay

HeLa cells were grown in 6 well plates (0.5×10^6 cells per well) for 24 h and were treated with and without IC_{50} concentration of compounds **3i, 3j** and **DOX** for 24 and 48 h. After treatment, cells were washed twice with phosphate buffer saline (PBS) and fixed with 4% paraformaldehyde at 4 °C for 10 min. Then, the cells were incubated with 0.5 mL of PBS solution containing mixture of acridine orange and ethidium bromide in dark for 10 min at 37 °C. The stained cells were washed with PBS to remove the excess dye and the cells were observed immediately under fluorescence microscope (Nikon, Eclipse, E 600).

4.2.5. Annexin-V (APC)/propidium iodide dual staining assay

HeLa cells at a density of 0.5×10^6 per plate were seeded overnight and treated with compounds **3i, 3j** and **DOX** at their IC_{50} concentration and harvested at scheduled time points post-treatment and re-suspended in 300 µL 1× binding buffer followed by incubation with 5 µL Annexin V and 5 µL propidium iodide for 20 min in dark. The samples were analyzed for Annexin V and PI binding by FACS calibur (Becton Dickinson) using Cell Quest pro software. Data was collected using logarithmic amplification of both the FL2 (PI) and FL4 (AV) channels. Quadrants of the dot plots were analyzed using the Cell Quest pro software. Unstained cells were used as control for auto-fluorescence. Cells stained alone with Annexin V or PI were used to adjust the photomultiplier voltages settings to eliminate spectral overlap between the FL2 and FL4 signals.

4.2.6. DNA fragmentation analysis

HeLa cells (0.5×10^6) were incubated for 24 h in medium containing 10% FBS. After 24 h cells were treated with IC_{50} concentration of **3i**, **3j** and **DOX**. After appropriate time points, cells were collected by trypsinization and rinsed twice in cold phosphate buffered saline (PBS, pH 7.4). Genomic DNA was extracted from HeLa cells using centrifuge protocol of AxyPrep Multisource Genomic DNA Miniprep Kit. Isolated DNA was analyzed by agarose gel electrophoresis.

4.2.7. Cell cycle analysis

Appropriate number of HeLa cells per plate was seeded overnight. Cells were then treated the next morning with test compounds **3i**, **3j** and positive control **DOX** and harvested after 24 h. Cell pellet was collected by centrifugation at 1100 rpm (Eppendorf, Centrifuge 5810 R) for 5 min followed by washing twice with PBS, and fixing cells was observed in inverted phase contrast microscope (Nikon, Eclipse TE 2000, Japan) after 24 and 48 h of treatment at a focus of 10× and the images were captured using NIS elements software.

4.2.8. Western blot analysis

Following appropriate treatment with test compounds **3i** and **3j**, cells were detached from the substrate and collected by centrifugation (1500 rpm, 5 min, 4 °C). The pellets were washed with ice cold PBS and re-suspended in RIPA buffer (Cell Signaling Technology, MA, US). Total protein was then collected by centrifugation of sample at 12,000*g* for 30 min at 4 °C and quantified using Bradford Protein Estimation kit (Genei, Banglore, India). Cell lysates were diluted with 2× Laemmli sample buffer, and then heated at 95–100 °C for 5 min. Equal amount of protein (50 μg) was loaded and resolved using 10–16% SDS-PAGE and transferred onto PVDF membrane (MDI, Ambala, India). Blots were blocked overnight at 4 °C in PBS-Tween 20 (0.05%)-BSA (5%) and then incubated with primary antibodies (caspase 3, PARP, Bcl-2, Bax, cyclin B1, p21 and β-actin) in blocking buffer overnight at 4 °C. This was followed by incubation with horseradish peroxidase–conjugated secondary antibody for 3 h at room temperature. Immunoreactive bands were probed with the enhanced chemiluminiscence (ECL) western blot detection system (Biogene, India) according to manufacturer's instructions and viewed in gel documentation system LAS4000 (FUJIFILM, USA).

4.2.9. Statistical analysis

The values were recorded as mean ± SD. The data were analyzed by using one way ANOVA test; differences below the 0.001 level ($P < 0.05$) were considered as statistically significant.

Conflict of interest

All authors declare no conflicts of interest.

Acknowledgements

Nalini Yadav would like to acknowledge Lady Tata Memorial Trust, Mumbai, India for providing the fellowship for conducting the research work. All the authors would like to acknowledge University Scientific Instrumentation Centre, Delhi University for providing NMR and IR facilities, Sophisticated Analytical Instrumentation Facility, Central Drug Research Institute, Lucknow for providing HRMS facility.

Appendix A. Supplementary data

Supplementary data associated with this article can be found, in the online version, at http://dx.doi.org/10.1016/j.biopha.2017.08.110.

References

[1] S. Eckhardt, Recent progress in the development of anticancer agents, Curr. Med. Chem.-Anti-Cancer Agents 2 (3) (2002) 419–439.
[2] Annex A. 2.1 Global patterns of health risk.
[3] B.W. Stewart, P. Kleihues, World Cancer Report, IARC press, Lyon, 2003.
[4] A. Boutayeb, S. Boutayeb, The burden of non communicable diseases in developing countries, Int. J. Equity Health 4 (1) (2005) 2.
[5] I. Khanna, Drug discovery in pharmaceutical industry: productivity challenges and trends, Drug Discov. Today 17 (19) (2012) 1088–1102.
[6] G. Moghaddam, S.A. Ebrahimi, N. Rahbar-Roshandel, A. Foroumadi, Antiproliferative activity of flavonoids: influence of the sequential methoxylation state of the flavonoid structure, Phytother. Res. 26 (7) (2012) 1023–1028.
[7] S.X. Cai, B. Nguyen, S. Jia, J. Herich, J. Guastella, S. Reddy, et al., Discovery of substituted N-phenyl nicotinamides as potent inducers of apoptosis using a cell-and caspase-based high throughput screening assay, J. Med. Chem. 46 (12) (2003) 2474–2481.
[8] B.S. Holla, R. Gonsalves, S. Shenoy, Synthesis and antibacterial studies of a new series of 1, 2-bis (1, 3, 4-oxadiazol-2-yl) ethanes and 1, 2-bis (4-amino-1, 2, 4-triazol-3-yl) ethanes, Eur. J. Med. Chem. 35 (2) (2000) 267–271.
[9] F. Macaev, G. Rusu, S. Pogrebnoi, A. Gudima, E. Stingaci, L. Vlad, et al., Synthesis of novel 5-aryl-2-thio-1, 3, 4-oxadiazoles and the study of their structure–anti-mycobacterial activities, Bioorg. Med. Chem. 13 (16) (2005) 4842–4850.
[10] F. Liu, X.-Q. Luo, B.-A. Song, P.S. Bhadury, S. Yang, L.-H. Jin, et al., Synthesis and antifungal activity of novel sulfoxide derivatives containing trimethoxyphenyl substituted 1, 3, 4-thiadiazole and 1, 3, 4-oxadiazole moiety, Bioorg. Med. Chem. 16 (7) (2008) 3632–3640.
[11] A.A. El-Emam, O.A. Al-Deeb, M. Al-Omar, J. Lehmann, Synthesis, antimicrobial, and anti-HIV-1 activity of certain 5-(1-adamantyl)-2-substituted thio-1, 3, 4-oxadiazoles and 5-(1-adamantyl)-3-substituted aminomethyl-1, 3, 4-oxadiazoline-2-thiones, Bioorg. Med. Chem. 12 (19) (2004) 5107–5113.
[12] M.M. Burbuliene, V. Jakubkiene, G. Mekuskiene, E. Udrenaite, R. Smicius, P. Vainilavicius, Synthesis, anti-inflammatory activity of derivatives of 5-(2-disubstitutedamino-6-methyl-pyrimidin-4-yl)-sulfanylmethyl-3 H-1, 3, 4-oxadiazole-2-thiones, Il Farmaco 59 (10) (2004) 767–774.
[13] E. Palaska, G. Şahin, P. Kelicen, N.T. Durlu, G. Altinok, Synthesis and anti-inflammatory activity of 1-acylthiosemicarbazides, 1, 3, 4-oxadiazoles, 1, 3, 4-thiadiazoles and 1, 2, 4-triazole-3-thiones, Il Farmaco 57 (2) (2002) 101–107.
[14] M. Akhter, A. Husain, B. Azad, M. Ajmal, Aroylpropionic acid based 2, 5-disubstituted-1, 3, 4-oxadiazoles: synthesis and their anti-inflammatory and analgesic activities, Eur. J. Med. Chem. 44 (6) (2009) 2372–2378.
[15] K.G. Liu, J.S. Smith, A.H. Ayscue, B.R. Henke, M.H. Lambert, L.M. Leesnitzer, et al., Identification of a series of oxadiazole-substituted α-isopropoxy phenylpropanoic acids with activity on PPARα, PPARγ, and PPARδ, Bioorg. Med. Chem. Lett. 11 (17) (2001) 2385–2388.
[16] A. Zarghi, S.A. Tabatabai, M. Faizi, A. Ahadian, P. Navabi, V. Zanganeh, et al., Synthesis and anticonvulsant activity of new 2-substituted-5-(2-benzyloxyphenyl)-1, 3, 4-oxadiazoles, Bioorg. Med. Chem. Lett. 15 (7) (2005) 1863–1865.
[17] D. Kumar, S. Sundaree, E.O. Johnson, K. Shah, An efficient synthesis and biological study of novel indolyl-1, 3, 4-oxadiazoles as potent anticancer agents, Bioorg. Med. Chem. Lett. 19 (15) (2009) 4492–4494.
[18] M.A. Abdel-Aziz, K. Metwally, A.M. Gamal-Eldeen, O. M Aly, 1,3,4-oxadiazole-2-thione derivatives; novel approach for anticancer and tubulin polymerization inhibitory activities, Anti-Cancer Agents Med. Chem. (Formerly Curr. Med. Chem.-Anti-Cancer Agents) 16 (2) (2016) 269–277.

[19] A.O. Maslat, M. Abussaud, H. Tashtoush, M. Al-Talib, Synthesis, antibacterial, antifungal and genotoxic activity of bis-1, 3, 4-oxadiazole derivatives, Pol. J. Pharmacol. 54 (1) (2002) 55–60.
[20] A.A. Farghaly, A.A. Bekhit, J. Young Park, Design and synthesis of some oxadiazolyl, thiadiazolyl, thiazolidinyl, and thiazolyl derivatives of 1 H-Pyrazole as anti-inflammatory antimicrobial agents, Arch. Pharm. 333 (2-3) (2000) 53–57.
[21] A. Andreani, M. Granaiola, A. Leoni, A. Locatelli, R. Morigi, M. Rambaldi, Synthesis and antitubercular activity of imidazo 2,1-b thiazoles, Eur. J. Med. Chem. 36 (9) (2001) 743–746.
[22] S. Dash, B.A. Kumar, J. Singh, B. Maiti, T. Maity, Synthesis of some novel 3, 5-disubstituted 1, 3, 4-oxadiazole derivatives and anticancer activity on EAC animal model, Med. Chem. Res. 20 (8) (2011) 1206–1213.
[23] S. Bondock, S. Adel, H.A. Etman, F.A. Badria, Synthesis and antitumor evaluation of some new 1, 3, 4-oxadiazole-based heterocycles, Eur. J. Med. Chem. 48 (2012) 192–199.
[24] M. Rashid, A. Husain, R. Mishra, Synthesis of benzimidazoles bearing oxadiazole nucleus as anticancer agents, Eur. J. Med. Chem. 54 (2012) 855–866.
[25] A.S. Aboraia, H.M. Abdel-Rahman, N.M. Mahfouz, M.A. El-Gendy, Novel 5-(2-hydroxyphenyl)-3-substituted-2, 3-dihydro-1, 3, 4-oxadiazole-2-thione derivatives: promising anticancer agents, Bioorg. Med. Chem. 14 (4) (2006) 1236–1246.
[26] J. Sun, H. Zhu, Z.-M. Yang, H.-L. Zhu, Synthesis, molecular modeling and biological evaluation of 2-aminomethyl-5-(quinolin-2-yl)-1, 3, 4-oxadiazole-2 (3 H)-thione quinolone derivatives as novel anticancer agent, Eur. J. Med. Chem. 60 (2013) 23–28.
[27] T. Mosmann, Rapid colorimetric assay for cellular growth and survival: application to proliferation and cytotoxicity assays, J. Immunol. Methods 65 (1-2) (1983) 55–63.
[28] A. Ahmad, H. Varshney, A. Rauf, A. Sherwani, M. Owais, Synthesis and anticancer activity of long chain substituted 1, 3, 4-oxadiazol-2-thione, 1, 2, 4-triazol-3-thione and 1, 2, 4-triazolo 3,4-b-1, 3, 4-thiadiazine derivatives, Arab. J. Chem. 10 (2) (2017) S3347–S3357.
[29] R. Gudipati, R.N.R. Anreddy, S. Manda, Synthesis, characterization and anticancer activity of certain 3-{4-(5-mercapto-1, 3, 4-oxadiazole-2-yl) phenylimino} indolin-2-one derivatives, Saudi Pharm. J. 19 (3) (2011) 153–158.
[30] R.B. Badisa, S.F. Darling-Reed, P. Joseph, J.S. Cooperwood, L.M. Latinwo, C.B. Goodman, Selective cytotoxic activities of two novel synthetic drugs on human breast carcinoma MCF-7 cells, Anticancer Res. 29 (8) (2009) 2993–2996.
[31] S.B. Bratton, G.M. Cohen, Apoptotic death sensor: an organelle's alter ego? Trends Pharmacol. Sci. 22 (6) (2001) 306–315.
[32] L.G. Rodriguez, X. Wu, J.-L. Guan, Wound-healing assay, Cell Migr. Dev. Methods Protoc. (2005) 23–29.
[33] D.H. Park, S.K. Kim, I.H. Shin, Y.J. Jeong, Electricity production in biofuel cell using modified graphite electrode with neutral red, Biotechnol. Lett. 22 (16) (2000) 1301–1304.
[34] D. Baskić, S. Popović, P. Ristić, N.N. Arsenijević, Analysis of cycloheximide-induced apoptosis in human leukocytes: fluorescence microscopy using annexin V/propidium iodide versus acridin orange/ethidium bromide, Cell Biol. Int. 30 (11) (2006) 924–932.
[35] N.M. Weir, K. Selvendiran, V.K. Kutala, L. Tong, S. Vishwanath, M. Rajaram, et al., Curcumin induces G2/M arrest and apoptosis in cisplatin-resistant human ovarian cancer cells by modulating Akt and p38 MAPK, Cancer Biol. Ther. 6 (2) (2007) 178–184.
[36] Q. Hou, T. Zhao, H. Zhang, H. Lu, Q. Zhang, L. Sun, et al., Granzyme H induces apoptosis of target tumor cells characterized by DNA fragmentation and Bid-dependent mitochondrial damage, Mol. Immunol. 45 (4) (2008) 1044–1055.
[37] S. Elmore, Apoptosis: a review of programmed cell death, Toxicol. Pathol. 35 (4) (2007) 495–516.
[38] S. Kalimuthu, K. Se-Kwon, Cell survival and apoptosis signaling as therapeutic target for cancer: marine bioactive compounds, Int. J. Mol. Sci. 14 (2) (2013) 2334–2354.
[39] D. McIlroy, H. Sakahira, R.V. Talanian, S. Nagata, Involvement of caspase 3-activated DNase in internucleosomal DNA cleavage induced by diverse apoptotic stimuli, Oncogene 18 (31) (1999) 4401–4408.
[40] A.H. Boulares, A.G. Yakovlev, V. Ivanova, B.A. Stoica, G. Wang, S. Iyer, et al., Role of poly (ADP-ribose) polymerase (PARP) cleavage in apoptosis Caspase 3-resistant PARP mutant increases rates of apoptosis in transfected cells, J. Biol. Chem. 274 (33) (1999) 22932–22940.
[41] D.G. Tang, A.T. Porter, Target to apoptosis: a hopeful weapon for prostate cancer, Prostate 32 (4) (1997) 284–293.
[42] J.C. Reed, Regulation of apoptosis by bcl-2 family proteins and its role in cancer and chemoresistance, Curr. Opin. Oncol. 7 (6) (1995) 541–546.
[43] K.T. Chan, F.Y. Meng, Q. Li, C.Y. Ho, T.S. Lam, Y. To, et al., Cucurbitacin B induces apoptosis and S phase cell cycle arrest in BEL-7402 human hepatocellular carcinoma cells and is effective via oral administration, Cancer Lett. 294 (1) (2010) 118–124.
[44] A.M. Hernandez, E.S. Colvin, Y.-C. Chen, S.L. Geiss, L.E. Eller, P.T. Fueger, Upregulation of p21 activates the intrinsic apoptotic pathway in β-cells, Am. J. Physiol.-Endocrinol. Metab. 304 (12) (2013) E1281–E1290.
[45] H.-W. Han, H.-Y. Qiu, C. Hu, W.-X. Sun, R.-W. Yang, J.-L. Qi, et al., Design, synthesis and anti-cancer activity evaluation of podophyllotoxin-norcantharidin hybrid drugs, Bioorg. Med. Chem. Lett. 26 (14) (2016) 3237–3242.